Synthesis and phase transformation studies of Nickel Cadmium Co-doped Bismuth Vandium Oxide

Faria K. Naqvi[a], and Saba Beg[a*]

[a] Solid–State Chemistry Lab, Physical Chemistry Division, Department of Chemistry, Aligarh Muslim University, Aligarh, INDIA 202002

Abstract: The new oxide ion conductor related to the BIMEVOX family, BINICDVOX has been synthesized in the composition range $0.05 \leq x \leq 0.20$, using the sol-gel reaction route. The highly conducting tetragonal γ-type is stabilized down to room temperature for the compositions $x \geq 0.17$. The conductivity and activation energies were calculated for all the synthesised samples, and it was found that as the thermal energy increases, the movement of oxide ion vacancy increases. The effect of the Ni-Cd double substitution on the electrical properties of $Bi_4V_2O_{11}$ has been studied and found that the electrical conductivity has been significantly increased for the compositions x = 0.17 and x = 0.20.

Keyword: *$BiVO_4$,*BINICDVOX, Sol-gel.

I.Introduction.

Solid oxide fuel cells (SOFCs) are one of the most promising energy conversion devices and have attracted considerable attention for their high conversion efficiency, fuel flexibility, and negligible environmental pollution [1,2]. Conventional SOFCs are typically operated in the temperature range of 800-1000 °C to achieve the desired properties. Such high operating temperatures lead to severe problems, such as the interfacial reaction between electrode and electrolyte, performance degradation of the SOFC components, and the resulting high cost of materials [3,4]. Hence it is desired to lower the operating temperature of the SOFCs to the intermediate-temperature (IT) range (600-800°C), that is, to develop the so-called IT-SOFCs. However, the performance of traditional cathode materials, such as $La_{1-x}Sr_xMnO_{3-\delta}$, decreases dramatically below 800 °C because of the poor oxygen ion conductivity and insufficient catalytic activity for the oxygen reduction reaction (ORR) [5,6]. Therefore, alternative cathode materials need to be developed with high electrocatalytic activity for ORR in IT-SOFCs.

Double perovskite, Bismuth Vanadate ($Bi_4V_2O_{11}$) is a layered Aurivillius compound of the general composition $[Bi_2O_2]^{2+}[A_{n-1}BnO_{3n+1}]^{2-}$ where n= 1. $Bi_4V_2O_{11}$ is characterized as intergrowth of two structural elements: fluorite-like $(Bi_2O_2)^{2+}$ bismuthate layers and oxygen-deficient perovskite $(VO_{3.5}\ \square_{0.5})^{2-}$ vanadate layers, where □ refers to the oxygen ion vacancies, which allow the charge carriers (oxygen ions) to diffuse through the lattice crystal, and 1/8 of the oxygen concentration of the perovskite vanadate layers is vacant [7]. Consequently, the increase in temperature is associated with an increase in the disordering of oxygen vacancies in the conducting vanadate layers $(VO_{3.5}\ \square_{0.5})^{2-}$.

$Bi_4V_2O_{11}$ displays two phase transformation α (monoclinic) ↔ β (orthorhombic) at 450 °C and β (orthorhombic) ↔ γ (tetragonal) at 570 °C. The disordering of oxygen vacancies in γ-$Bi_4V_2O_{11}$ is remarkably responsible for high and fascinating oxide ion conducting performance of γ-phase.

The γ phase is crystalline in the tetragonal space group (I4/mmm) [8]. It is stable above 570 °C, and can be preserved to room temperature by partial substitution of a wide variety of cations at vanadium site [8-20]. The partial substitution of cations for vanadium site suppresses the ordering of oxygen ion vacancies. Metal doped Bismuth Vanadium Oxides (BIMEVOXes) possess good oxide ion conductivity at intermediate temperatures, and hence can be used widely as solid electrolyte and cathode material in solid oxide fuel cells (SOFC), membrane for oxygen separation and oxygen catalytic dense membrane [1,21-22].The Nickel substituted bismuth vanadate $Bi_2Ni_{0.1}V_{0.9}O_{5.35}$ showed its high oxide ion conductivity in the range of (~ 1.71×10^{-3} S cm^{-1}) at 300 °C [23]. Lee et al. [24] reported the high ionic conductivity for Cadmium- substituted $Bi_4V_2O_{11}$ with composition $Bi_2Cd_{0.1-x}V_{0.9}O_{5.35}$ ~ 1.31×10^{-3} Scm^{-1} at 420 °C and 2.81×10^{-2} S cm^{-1} at 620 °C. This chapter presents the synthesis of the Nickle-Cadmium double substituted $Bi_4V_2O_{11}$ which leads to the formation of $Bi_2Ni_{0.1-x}Cd_xV_{0.9}O_{5.35-x/2-\delta}$ by using sol-gel reaction method, and study of the

phase structure of solid solutions by XRD, DTA and FT-IR. The electrical conductivity have been investigated by the AC impedance spectroscopy.

I. Experimental.

Samples of $Bi_2Ni_{0.1-x}Cd_xV_{0.9}O_{5.35-x/2-\delta}$in the composition range $0.05 \leq x \leq 0.20$ were prepared by using analytical grade $Bi(NO_3)_3.5H_2O$ (Sigma Aldrich, 99.9%), NH_4 (Merk, 99%) ,V_2O_5 (Sigma Aldrich, 99.9%), CdO (Merck, 99%) and NiO (Sigma Aldrich, 99.9%) as starting materials. The samples were synthesized by bottom up sol gel method. The sol–gel method is a convenient way to manufacture non–agglomerated particles, and also helps to reduce the sintering temperature. In this method, citric acid in 0.2 Molar concentration is prepared which is used as a chelating agent and this prepared solution is mixed with ethylene glycol mixture in volumetric ratio of 3:1. Under constant stirring, ammonia (NH_3) solution was added to maintain the neutrality of the sol. Finally, obtained xerogel was dried at 90 ^oC for 12 hours.

The dried xerogel was thoroughly mixed in an agate mortar for further homogenization and then thermally calcined in a muffle furnace at 650^oC for 48hrs. After the complete calcination, samples of BINICDVOX were pelletized into a cylindrical shape with constant dimensions (15 mm in diameter and 2.4 to 3.1 mm thickness) under isostatic pressure of 425 MPa (Spectra lab SL–89). The pellets were again sintered in air at 650 ^oC for 12hrs.

IV. Characterization Techniques:

I. Crystallography

Structural properties of the calcined samples of BINICDVOX system were characterized by the X– ray powder diffraction (XRPD) using a Philips PW 1050/30 X–Ray Diffractometer with CuKα radiation (λ=1.54060 Å). The diffracted beams were collected in a 2θ range 20–60^o with an increment of 0.020° at a scan rate of 32.8 seconds/ step. The hkl values and symmetry of γ-phase is compared with Powder X software program and standard JCPDS data.

II. Differential Thermal Analysis

The differential thermal analysis (DTA) measurements were carried out by Schimatzu SC–TA 60 Thermal Analyser. The powdered samples were heated from 40 °C to 740 ^oC at constant heating rate of 10 °C/min and the experiments were run in nitrogen atmosphere supplied at a flow rate of 100 ml/min.

III. FT-IR Spectroscopy

FT-IR spectra of the various samples were recorded using 10 % KBr (w/w) in transmittance mode at room temperature using Perkin Elmer Spectrophotometer over the spectral range (400-2000 cm^{-1}).

IV. Electrical Characterization

Electrical properties were measured by means of AC impedance spectroscopy using a Wayne Kerr 4100 LCR Meter operated in the frequency range 1Hz – 1MHz with an AC signal of ~ 50 mV. For AC impedance measurements, all the sintered pellets were made conducting by applying chemically pure silver paste on both pellet surfaces and finally fired at 650 ^oC for 12 hrs. The experiments were run in air at every 20 ^oC interval from 100 ^oC to 600 ^oC with a 20 min thermal equilibration before each measurement. Impedance spectra were subjected to non–linear least squares fitting using a Z view software program.

Calculation of conductivity and capacitance, of grain and grain boundary (C_g and C_{gb}) from the corresponding circuits for each sample can be obtained by following the equation;

$$\sigma = 1/(R_t \times (L/A)) \qquad (1)$$

where, L is the thickness of the sample (in cm); A the area of the contact between the sample pellet and the electrodes (in cm^2), and R_t is the total resistance (in ohm) obtained from the fitting procedure. The total resistances (R_t) can be calculated from the values of grain (R_g) and grain boundary (R_{gb}) resistances as follows;

$$R_t = R_g + R_{gb} \quad (2)$$

The capacitances ($C_g$and C_{gb}) at the grain and grain boundary can be obtained by the equation;

$$C_i = \frac{1}{R_i \omega_i} \quad (3)$$

where, C_i is the capacitance, R_i is the resistance and ω_i is the angular frequency at grain (i=g) and grain boundary (i=gb), calculated from the corresponding applied frequency at the maxima of the semicircle according to the equation;

$$\omega_i = 2\pi f_{max,i} \quad (4)$$

where, $f_{max,i}$ is the frequency at maxima of the grain (i = g) in the grain boundary (i = gb) semicircles, respectively.

3.2 Result and Discussion.

Figure 1depicts the variation in the high temperature powder X-ray diffraction (PXRD)patterns of x = 0.17 xerogel as a function of calcination temperature. The sample obtained after calcination at 350 °C for 5 hours was still found to be somewhat amorphous. At this temperature, the broad diffraction peaks at 2θ = 28.25° exhibit I4/mmm symmetry, characteristic to the tetragonal phase according to standard JCPDS data (089-0102). However, after calcination at 550 °C the sample was completely converted into a crystalline γ-phase. This can be attributed to the partial decomposition of citrate precursor because, in general, it was found that the increase in calcination temperature results in the formation of well-crystallized product [3,4].

The XRPD patterns at room temperature for various compositions of $Bi_2Ni_{0.1-x}Cd_xV_{0.9}O_{5.35-x/2-\delta}$ system is shown in Figure2. The tetragonal crystalline phase with (I4/mmm) space group is evidenced for the compositions x = 0.17 and 0.20, which can be demonstrated by the presence of the singlet diffraction peak (110) at 2θ ~ 32°. In the case of samples 0.05 ≤ x ≤ 0.13, the splitting in 110 peak occurring at 2θ ~ 32° gives doublet peaks indexed as (020) and (200) reflections towards higher 2θ values (Shown in figure 3a), shows the stabilization of the monoclinic α and orthorhombic β phase [19]. The stabilization of monoclinic symmetry α-phase for compositions x = 0.05 and 0.10 can be identified by the existence of two doublets, at 2θ ~ 32° and 2θ = 45 - 46°, due to splitting of the (110) and (220) reflections, respectively [4,18].

Diffraction pattern of Nickel and Cadmium co-doped bismuth vanadium oxide at different concentrations exhibits a monoclinic scheelite α phase according to standard JCPDS data (014-0688) for the compositions x = 0.05 and 0.10. It has been noticed that the highly intense diffraction peak (121) corresponding to the Nickel-Bismuth vanadium oxide samples shifts to higher 2θ angle compared to parent compound bismuth vanadium oxide as shown in the figure 3b. This shift occurs from the structural disorders such as compressive strains due to the incorporation of Nickel/Cadmium into the crystal sites of bismuth vanadium oxide structure [9-11]. For compositions with x ≤ 0.10, a characteristic intense doublet peak is observed at 2θ= 46.5 ascribed to (026) and (606) which depicts the presence of monoclinic α-phase as that of the parent compound. For x ≥ 0.17, the intensity of the peak gets lowered to smaller 2θ value showing the presence of tetragonal γ-phase of higher symmetry. However, the tetragonal γ-phase is stabilized for x ≥ 0.17 as clearly evidenced by the presence of a singlet sub lattice (110) at 32.2°. The intensity of the lines depend on the arrangement of atoms in the unit cell. The decrease in the intensity and the increase in the FWHM of the diffraction lines can be induced by the disorder in the location of Nickel and Cadmium in bismuth vanadium oxide layers or may be due to size differences between substituted ions and the vanadium.

$$D = \frac{0.9\lambda}{\beta \cos\theta} \quad (1)$$

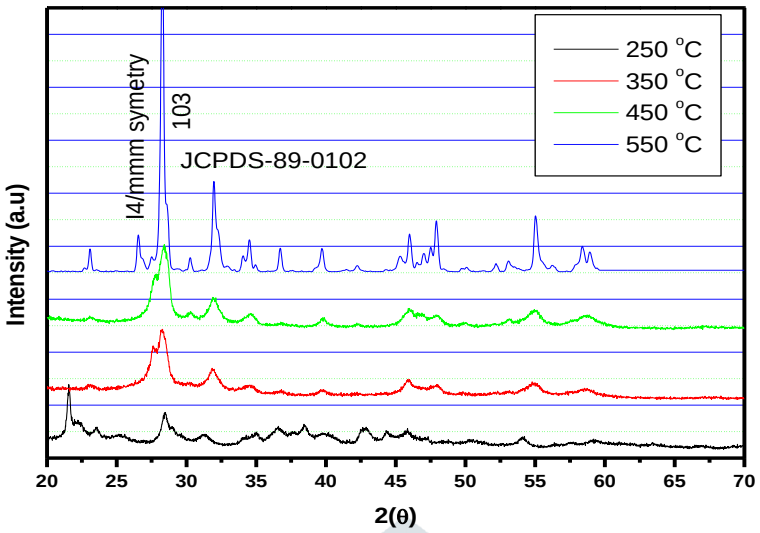

Figure 1: PXRD patterns of x = 0.17 xerogel calcinated at different temperatures.

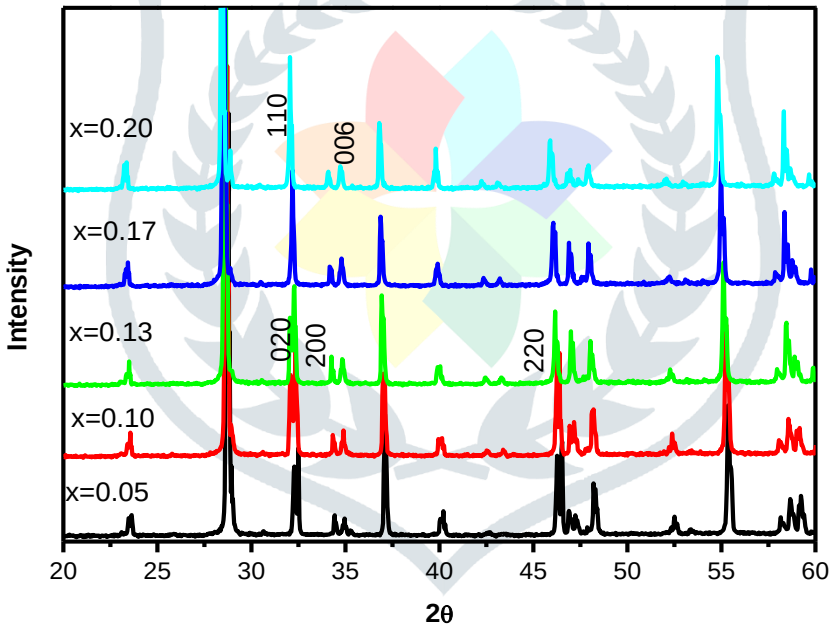

Figure 2: PXRD patterns of $Bi_2Ni_{0.1-x}Cd_xV_{0.9}O_{5.35-x/2-\delta}$ system of composition $0.05 \leq x \leq 0.20$.

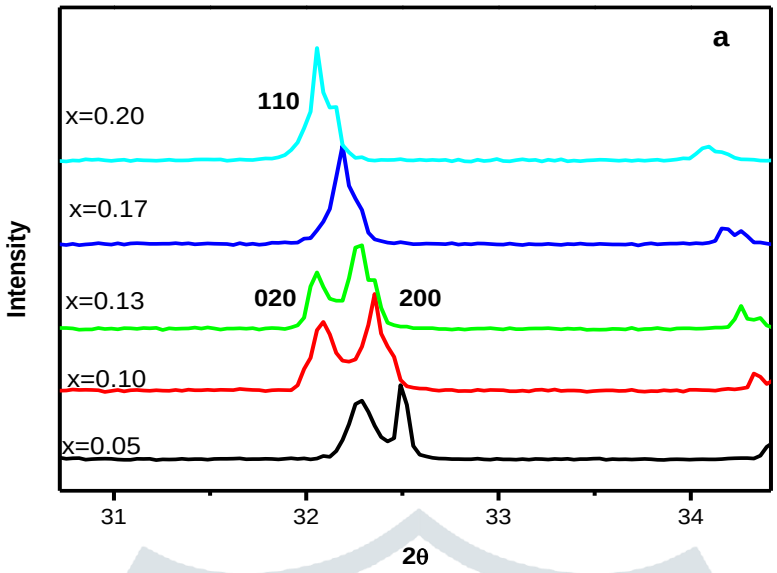

Fig. 3a: Enlarged PXRD patterns at 2θ = 31- 35° of $Bi_2Ni_{0.1-x}Cd_xV_{0.9}O_{5.35-x/2-\delta}$ system of composition 0.05≤ x ≤0.20

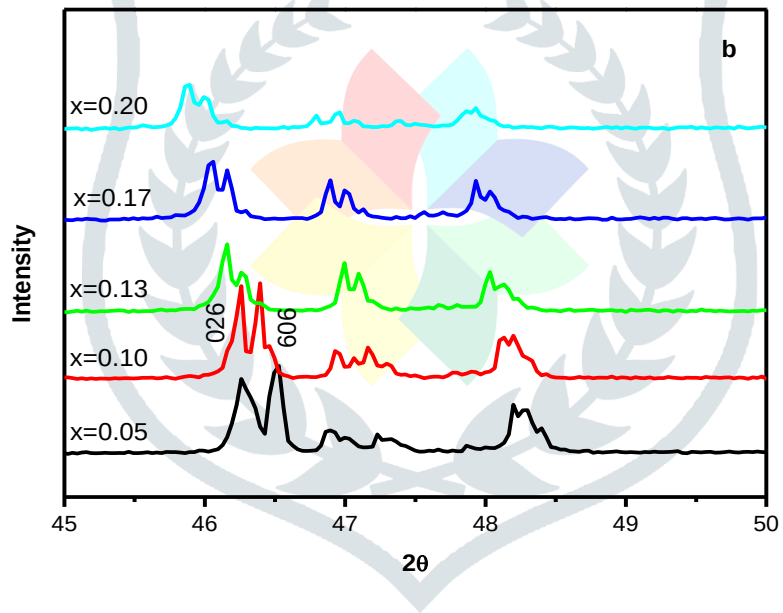

Fig.3b: Enlarged PXRD patterns at 2θ = 45-50° of $Bi_2Ni_{0.1-x}Cd_xV_{0.9}O_{5.35-x/2-\delta}$ system of composition 0.05≤ x ≤0.20

DTA curves obtained on heating run for $Bi_2Ni_{0.1-x}Cd_xV_{0.9}O_{5.35-x/2-\delta}$ samples with heating rate 10 °C/min are shown in Figure 4. A noticeable change in phase transition is observed with increase in Cd substitution. The small endothermic event around 480°C is associated with oxygen vacancies order-disorder transition for composition $x \geq 0.17$ which is also found in the other members of BIMEVOX [4,9]. For β phase sample, x = 0.13 the DTA curve showed the endothermic peak around 446 °C that is consistent with β to γ phase transition. Finally, the two endothermic peaks detected for samples with $0.05 \leq x \leq 0.10$ are associated with α to β phase and for composition $x \geq 0.13$ β to γ phase transitions are observed.

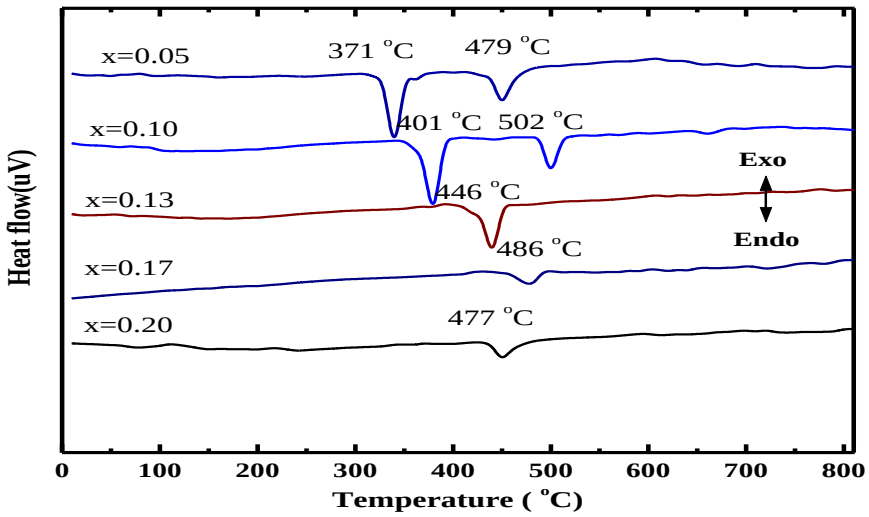

Figure 4: DTA thermograms for compositions 0.05 ≤ x ≤ 0.20 of BINICDVOX system.

FT-IR spectroscopy is used to characterize the different phase structures within the $Bi_2Ni_{0.1-x}Cd_xV_{0.9}O_{5.35-x/2-\delta}$ system. The FT-IR spectra for the compositions with 0.05≤x ≤0.20 and are illustrated in the Figure 5. The FT-IR spectra for the sample x = 0.17, γ polymorph shows the disappearance of fine structure in the FT-IR band between 600 and 1000 cm^{-1}[9, 10]. For composition x = 0.05 and 0.10, the ordered α phase can be characterized by the presence of fine structure in the FT-IR spectra which associates to ordering of the oxygen vacancies in vanadate layer. The more intense fine structure of FT-IR bands for x = 0.05 is associated with stabilization of ordered α monoclinic phase to room temperature. The intensity of fine structure of FT-IR bands in the range 600-1000 cm^{-1} for as x = 0.05 is lower than the composition x = 0.10.The composition, x = 0.17 is showing lower peak intensity in the FT-IR band between 600 and 1000 cm^{-1} if compared with compositions x = 0.05 and 0.10. This difference in peak intensity is due to the stabilization of γ, β and α phases for compositions x = 0.17, x = 0.13 and x = 0.05 respectively [10].

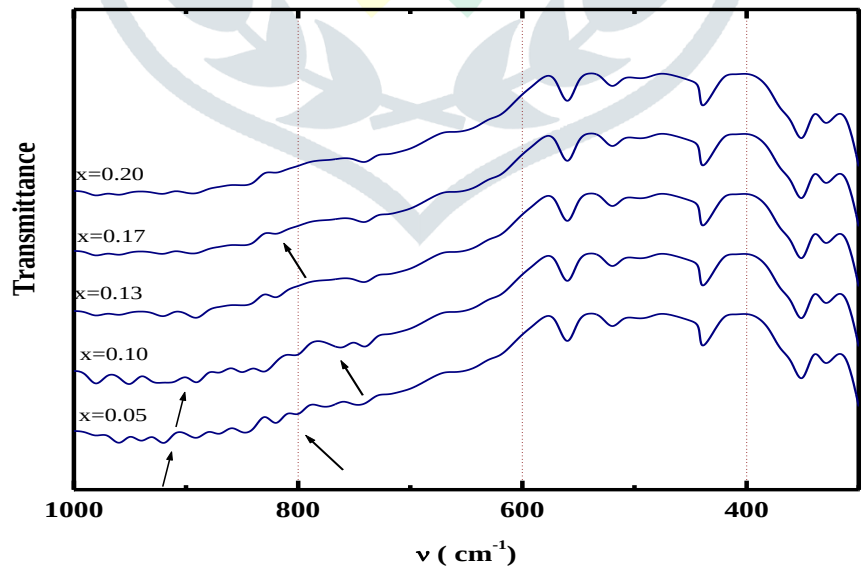

Figure 5: FT-IR spectra for compositions 0.05 ≤ x ≤ 0.20 of BINICDVOX system.

Figure 6 presents the typical complex impedance plane plot (Z″ vs. Z′) over a range of frequencies from 20 Hz to 1 MHz for sintered pellets of the $Bi_2Ni_{0.1-x}Cd_xV_{0.9}O_{5.35-x/2-\delta}$ system for compositions 0.05 ≤ x ≤ 0.20 at various temperatures 200 °C, 260 °C, 300°C and 380 °C. Representative Nyquist plots of complex impedance spectra are characterized by two semicircle arcs with centres located below line of real part of impedance Z′ that are associated with double-parallel resistance-capacitance (R-C)

contributions. The large impedance semicircle associated with the oxide ion transport through the grain, which is located at high frequency portion, arises from grain resistor R_g and grain capacitor C_g in parallel. The small impedance semicircle at lower frequency reflects the contribution of grain boundary impedance to conductivity of $Bi_2Ni_{0.1-x}Cd_xV_{0.9}O_{5.35-x/2-\delta}$ solid electrolyte, which represents the blocking effect of charge carrier by grain boundary. The effect of polarization at electrolyte-electrode interface appears as well-defined line inclined at an angle ~ 45° at lower frequency. This line inclined reflects that the charge carriers are oxide ion in nature [11].

The resistance of grain R_g is extracted from the intercept of high-frequency impedance semicircle with the real part of impedance Z'. The resistance of grain boundary R_{gb} is extracted from the intercept of low-frequency impedance semicircles with the real part of impedance Z'. The total resistance is estimated from the resistance of grain R_g and the resistance of grain boundary R_{gb} as,

$$R_t = R_g + R_{gb} \qquad (5)$$

As temperature increases, the intercept on the Z'-axis shifts towards the origin, reflecting an increase in conductivity [25]. The impedance semicircles are fitted to modeled electrical circuits consisting of two RC components (R_g // C_g) and (R_{gb} // C_{gb}) connected in series [26]. The resistances of grain R_g and grain boundary R_{gb} significantly change with the substitution of Cadmium. For composition x = 0.17, low values of resistance of bulk grain, R_g and grain boundary, R_{gb} are found as expected for highly conductive tetragonal γ phase demonstrated by XRD analysis. It can be seen, that as the temperature increases, the impedance decreases indicating that the resistance of grain response. The complex plane plots of impedance for the investigated samples show behaviour typical for the oxygen– conducting BIMEVOX family. For the composition x = 0.17, two separate semicircles are seen in the high and low– frequency regions, which are respectively assigned to grain and grain boundary contributions. The impedance of the electrode–electrolyte interface is clearly represented by the inclined spikes appearing at very low frequencies [27–29]. These impedance plots were well–modelled by the equivalent electrical circuits reported for the BINBVOX system [30].

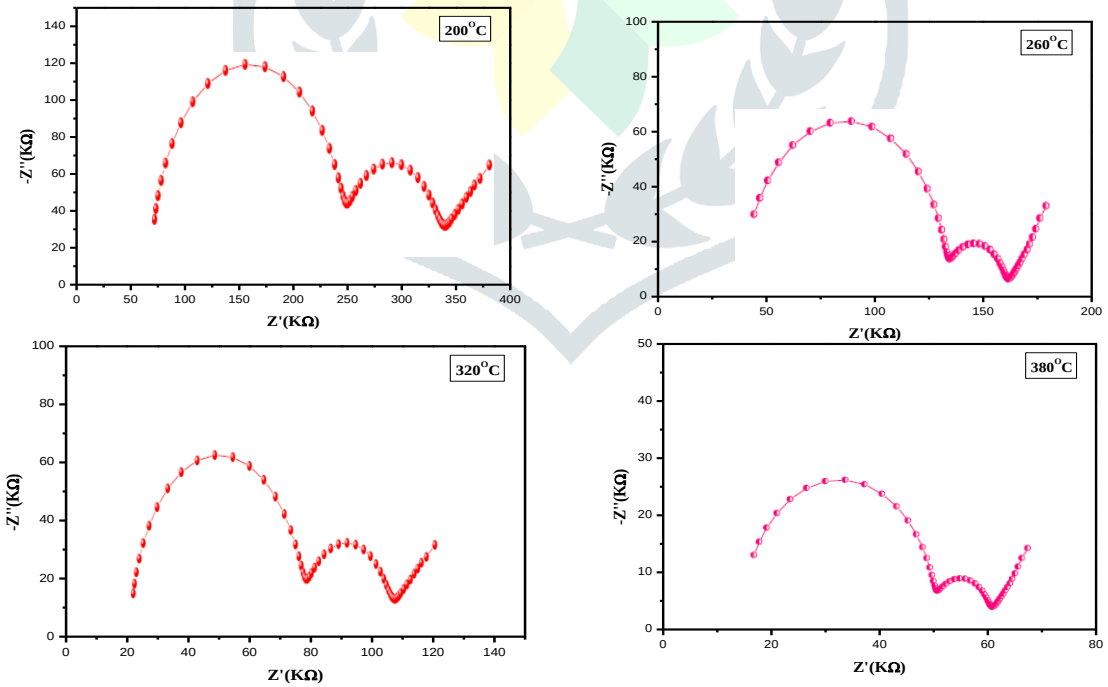

Fig. 6: Complex Impedance plane plots at four different temperatures for x=0.17 of BINICDVOX system

Table 1 represents the values of equivalent circuit parameters for both grain and grain boundary contribution estimated from the impedance plane plots for x = 0.17 at four different temperatures. It can be found that the grain contribution to the oxide–

ionic conductivity is more pronounced than that of the grain boundary contribution, because the values of R_g are higher than R_{gb}. It can also be noticed that the reduction in R_g values is faster than R_{gb} with increasing temperature. Moreover, the values of C_{gb} are higher than that of C_g which suggests that the permittivity increases with the accumulation of charge carriers at the grain boundary. The highest values of capacitances C_g and C_{gb} are found to be 2.47×10^{-4} and 4.78×10^{-4}F respectively at 380°C, suggesting more polarizability of the sample at this temperature. Hence, the total electrical permittivity of the sample is mainly attributed to the increased charge accumulation at the grain boundaries [27-29]. The capacitance value can be calculated using the following equation ($2\pi f_{top}RC=1$) where, $2\pi f_{top}$ is the angular frequency at the top of semicircle arc ($\omega_{top} = 2\pi f_{top}$). As temperature increases, the resistance of grain and grain boundary decreases significantly due to the increase of the charge carrier concentration and decreasing time constant of oxide ion diffusion through grain and grain boundary.

Table 1: AC impedance plane plots of BINICDVOX system for composition x=0.17 at four different temperatures.

T (ºC)	R_g(kΩ)	C_g(F)	R_{gb}(kΩ)	C_{gb}(F)	R_t(kΩ)
200	204.96	5.11×10^{-6}	85.55	6.79×10^{-6}	290.51
260	77.85	2.7×10^{-5}	38.81	3.08×10^{-5}	116.66
320	56.23	5.21×10^{-5}	26.99	5.89×10^{-5}	83.22
380	24.08	2.47×10^{-4}	12.43	4.78×10^{-4}	36.51

The separation of oxide ion diffusion process in inter particle interaction such as grain and grain boundary is possible in the complex impedance spectra of $Bi_2Ni_{0.1-x}Cd_xV_{0.9}O_{5.35-x/2-\delta}$ solid electrolyte for temperatures below ~ 450 °C, so that the total resistance of solid electrolyte is computed as resistance of grain R_g and resistance of grain boundary R_{gb} ($R_t = R_g + R_{gb}$). At temperatures above 600 °C, the semicircle arc vanishes because of shifting of semicircles to higher frequency side and only the line inclined appears due to the limited maximum frequency range of LCR (1 MHz), which is not enough to characterize the complex impedance plane plot at higher temperature. The total resistance is calculated from the intersect of the line inclined with the real part of impedance Z′ (R_t = Z′ intercept) [8,31]. The shifting of spike line, associated with polarization of electrode, with temperature is increased toward the lower value of resistance (i.e. Z′) indicating that the conduction property increases.

The total ionic conductivity can be calculated using the equation $\sigma = L/(R_t.A)$ where L/A is thickness /cross sectional area ratio of sintered pellets. The temperature dependence of total ionic conductivity for all studied compositions of $Bi_2Ni_{0.1-x}Cd_xV_{0.9}O_{5.35-x/2-\delta}$ system is displayed in figure 7. Characteristically, the break in the two regions in the Arrhenius plot (log σ T vs. 1/T) for composition x = 0.17 has been observed. Each line has different slope and activation energy, but with discontinuity at temperature between 450-500 °C, which indicates the phase transition.

The change in the slope at the Arrhenius plot is associated with β to γ phase transition due to the change of ordering of oxygen vacancies in vanadate perovskite layer from low temperature ordered oxygen vacancies (β) to high temperature disordered oxygen vacancies (γ). For compounds $0.05 \leq x \leq 0.13$ the conductivity behaviour are noticed as two linear regions in the Arrhenius plot, low temperature linear region corresponding to α polymorph (150-450 °C) and high temperature linear region corresponding to β polymorph (500- 700 °C) which is well separated below and above 450 °C. The conductivity behaviour clearly evidences the stabilization of β orthorhombic phase with β to γ phase transitions. At high substitution level of Ni by Cd for compositions, $0.05 \leq x \leq 0.20$, the Arrhenius plot is characterized by three linear regions with different slopes that demonstrate the stabilization of α

monoclinic phase. It is interesting to note that the Arrhenius plot demonstrates the phase transition as a function of temperature and composition in the $Bi_2Ni_{0.1-x}Cd_xV_{0.9}O_{5.35-x/2-\delta}$ system.

The conductivity vs temperature plot for x=0.17 is shown in figure 8. This figure clearly reveals that the conductivity increases with increase in temperature.

The activation energy of low-temperature region E_{LT} and high-temperature region E_{HT} is calculated from the slope of linear least square fitting of Arrhenius dependence $\sigma T = Aexp(-Ea/kT)$ in the low-temperature region (150°C – 450°C) and high-temperature region (500 °C- 700 °C). The tetragonal high-temperature disordered (γ) phase has a lower value of activation energy, due to the disordering of oxide ion vacancies in the tetragonal γ phase.

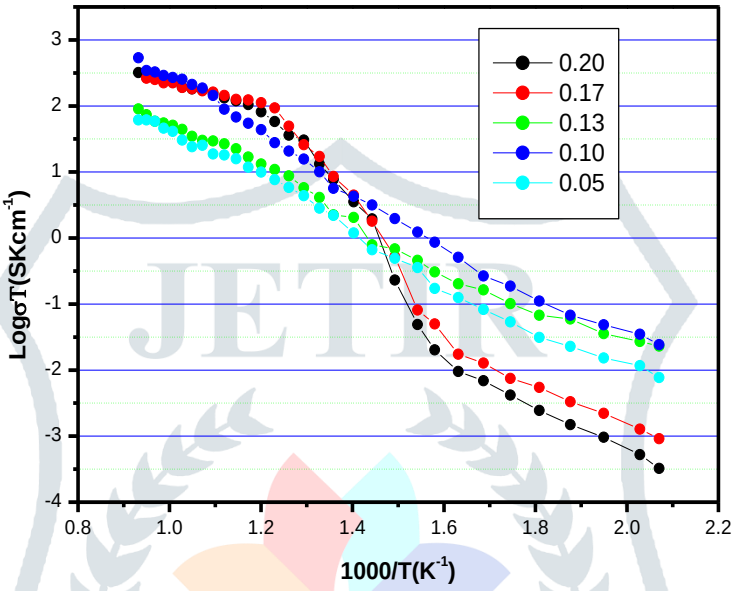

Figure 7: Arrhenius plot for total ionic Conductivity of BINICDVOX system

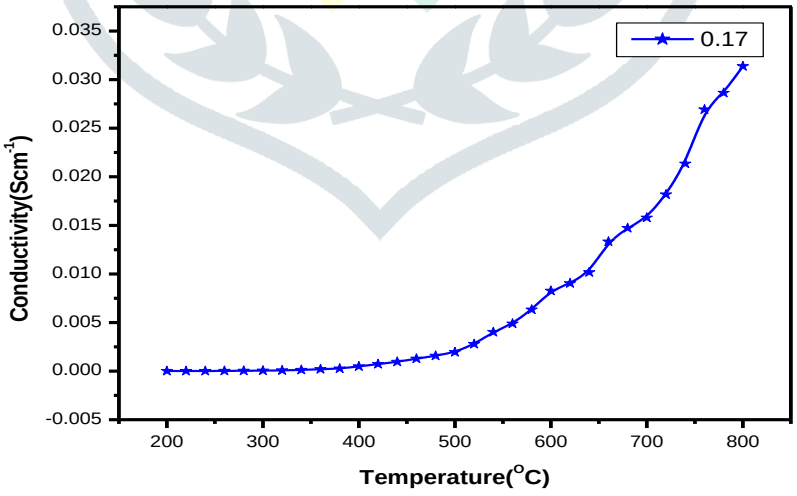

Figure 8: Conductivity vs Temperature plot for x=0.17 composition.

The lower values of oxide ion conduction are associated with higher values of activation energy of ordered monoclinic (α) and orthorhombic (β) phases. The lower values of conduction activation energy accompanied with higher oxide ion conductivity for the disordered high-temperature tetragonal (γ) phase. This is due to the fully disordering of oxygen vacancies in the vanadate layer for the γ phase that leads to lower energy required for oxide ion migration through the more disordered crystal lattice. (Table2).

Table 2: Values of Electrical Conductivity and Activation Energies

Compositions	ΔE_{LT}(eV)	σ_{300}(Scm^{-1})	ΔE_{HT}(eV)	σ_{600}(Scm^{-1})
0.05	0.88	1.04×10^{-4}	0.37	0.071
0.10	0.87	2.01×10^{-4}	0.34	0.066
0.13	0.64	2.5×10^{-4}	0.35	0.061
0.17	0.37	3.2×10^{-3}	0.33	0.056
0.20	0.93	3.5×10^{-3}	0.32	0.043

5. Conclusions

The new oxide ion conductor related to the BIMEVOX family, BINICDVOX has been synthesized in the composition range $0.05 \leq x \leq 0.20$, using the sol-gel reaction route. The highly conducting tetragonal γ-type is stabilized down to room temperature for the compositions $x \geq 0.17$. The conductivity and activation energies were calculated for all the synthesised samples, and it was found that as the thermal energy increases, the movement of oxide ion vacancy increases. The effect of the Ni-Cd double substitution on the electrical properties of $Bi_4V_2O_{11}$ has been studied and found that the electrical conductivity has been significantly increased for the compositions x = 0.17 and x = 0.20.

Acknowledgement

We are grateful to the Chairperson, Department of Chemistry, Aligarh Muslim University Aligarh, for providing requisite research facilities. We would also like to express our sincere gratitude to CSIR for SRF fellowship File No. 09/112(0612)2K19 EMR-1.

References

[1] F. Abraham, M.F. Debreuille-Gresse, G. Mairesse, G. Nowogrocki, *Solid State Ionics* **28-30** (1988)529.

[2] I. Abrahams, F. Krok, *J. Mater. Chem.* **12** (2002) 3351.

[3] F. Abraham, J.C. Boivin, G. Mairesse, G. Nowogrocki, *Solid State Ionics* **40/41** (1990) 934.

[4] F. Krok, W. Bogusz, W. Jakubowski, J.R. Dygas, D. Bangobango, *Solid State Ionics* **70/71** (1994) 211.

[5] C.K. Lee, A.R. West, *Solid State Ionics* **86-88** (1996) 235.

[6] S. Beg, N. A.S. Al-Areqi, *J. Physics and Chemistry of Solids* **70** (2009) 1000.

[7] R.N. Vannier, G. Mairesse, F. Abraham, G. Nowogrocki, *Solid State Ionics* **70/71** (1994) 248.

[8] M.H. Paydar, A.M. Hadian, G. Fafilek, *J. Materials Science* **39** (2004) 1357.

[9] M. Alga, A. Ammar, B. Tanouti, A. Outzourhit, F, Mauvy, R. Decourt, *J. Solid State Chemistry* **178** (2005) 2873.

[10] S. Beg S, N.A.S. Al-Areqi, S. Haneef, *Solid State Ionics* **179** (2008) 2260.

[11] R. Gerhardt, *J. Phys. Chem. Solids* **55** (1994) 1491.

[12] M.H. Paydar, A.M. Hadian, G. Fafilek, *J. European Ceramic Society* **21** (2001) 1821.

[13] M. Alga, A. Ammar, R. Essalim, B. Tanouti, A. Outzourhit, F. Mauvy, R. Decourt, *Ionics* **11** (2005) 81.

[14] A. Al-Alas, S. Beg, N. A.S. Al-Areqi, S. Hafeez, *J. European Ceramic Society* **33** (2013) 2111.

[15] E.S. Buyanova, M.V. Morozova, Ju.V. Emelyanova, S.A. Petrova, R.G. Zakharov, N.V. Tarakina, V.M. Zhukovskiy, *Solid State Ionics* **243** (2013) 8.

[16] Yu-ki Taninouchi, Tetsuya Uda, Tetsu Ichitsubo, Yasuhiro Awakura, Eiichiro Matsubara, *Solid State Ionics* **181** (2010) 719.

[17] R. Chockalingam, S. Basu, *International Journal of Hydrogen Energy* **36** (2011) 14977.

[18] J.R. Dygas, F. Krok, W. Bogusz, P. Kurek, K. Reiselhuber, M.W. Breiter, *Solid State Ionics* **70/71** (1994) 239.

[19] C. Pirovano, M.C. Steil, E. Capoen, G. Nowogrocki, R.N. Vannier, *Solid State Ionics* **176** (2005) 2079.

[20] X. Guo, Y. Ding, *J. Electrochemical Society* **151** (2004) J1.

[21] M.M.E. Jacob, S. Rajendran, R. Gangadharan, M. Siluvai Michael, S.R. Sahaya Prabaharan, *Solid State Ionics* **86-88** (1996) 595.

[22] S. Beg, N.A.S. Al-Areqi, A. Al-Alas, *J. Alloys and Compounds* **479** (2009) 107.

[23] K.C. Anjaneya, G.P. Nayaka, J. Manjanna, G. Govindaraj, K.N. Ganesha, *J. Alloys and Compounds* **578** (2013) 53.

[24] M.C. Steil, F. Ratajczak, E. Capoen, C. Pirovano, R.N. Vannier, G. Mairesse, *Solid State Ionics* **176** (2005) 2305.

[25] K.M. Batoo, S. Kumar, C.G. Lee, Alimuddin, *Current Applied Physics* **9** (2009) 1397.